FINE STRUCTURE OF THE THERMAL AND NON-THERMAL X-RAYS IN THE SN 1006 SHELL

A. Bamba[1], R. Yamazaki[1], M. Ueno[1], and K. Koyama[1]

[1]*Department of Physics, Kyoto University, Kitashirakawa, Sakyo-ku, Kyoto, 606-8502, Japan*

ABSTRACT

The north east shell of SN 1006 is the most probable acceleration site of high energy electrons (up to $\sim$ 100 TeV) with the Fermi acceleration mechanism at the shock front. We resolved non-thermal filaments from thermal emission in the shell with the excellent spatial resolution of *Chandra*. The non-thermal filaments seem thin sheets with the scales of $\sim$ 1 arcsec (0.01 pc) and $\sim$ 20 arcsec (0.2 pc) at upstream and downstream, respectively. In a simple diffusive shock acceleration (DSA) model with the magnetic field parallel to the shock normal, the downstream region should have highly disordered magnetic field of 30–40 μG. The width at the upstream side is extremely small, comparable to the gyro-radius of the maximum energy electrons. This result is hard to be explained by a conventional DSA with the magnetic field parallel to the shock normal, hence require unusual conditions like perpendicular field at upstream and/or a new acceleration mechanism of electrons.

INTRODUCTION

Since the discovery of cosmic rays, the origin and acceleration mechanism up to $10^{15.5}$ eV (the "knee" energy) have been long-standing problems. A breakthrough came from the X-ray studies of SN 1006; Koyama et al. (1995) discovered synchrotron X-rays from the shells of this SNR, indicating the existence of extremely high energy electrons up to TeV or more produced by the first order Fermi acceleration.

The mechanism of the cosmic ray acceleration has also been studied for a long time and the most plausible process is a diffusive shock acceleration (DSA) (e.g. Bell 1978). Apart from the globally successful picture of DSA, detailed but important processes, such as the injection and the reflection of accelerated particles, have not yet been well understood. The spatial distribution of accelerated particles responsible for the non-thermal X-rays, may provide key information on these unclear processes. Previous observations, however, are limited in spatial resolution for a detailed study on the structure of shock acceleration process and injection efficiency. Although many observations and theoretical models are made for SN 1006, these problems are still open issue (e.g. Reynolds 1998).

In this paper, we report on the first results of the spectral and spatial studies on the non-thermal shock structure in the NE shell of SN 1006 with *Chandra*. We discuss the spectral analyses and determine the scale lengths of the structures for non-thermal electrons on the base of a simple and conventional DSA. In this paper, we assume the distance of SN 1006 to be 1.8 kpc (Green 2001).

OBSERVATION

We used the *Chandra* archival data of the ACIS on the NE shell of SN 1006 (Observation ID = 00732) observed on July 10–11, 2000 with the targeted position at (RA, DEC) = ($15^{\rm h}03^{\rm m}51^{\rm s}.6$, $-41^{\rm d}51^{\rm m}18^{\rm s}.8$). The satellite and instrument are described by Weisskopf et al. (1996). CCD chips I2, I3, S1, S2, S3, and S4 were used with the pointing center on S3. Data acquisition from the ACIS was made in the Timed-Exposure Faint mode with the readout time of 3.24 s. The data reductions and analyses were made using the *Chandra* Interactive Analysis of Observations (CIAO) software version 2.2.1. Using the Level 2 processed events

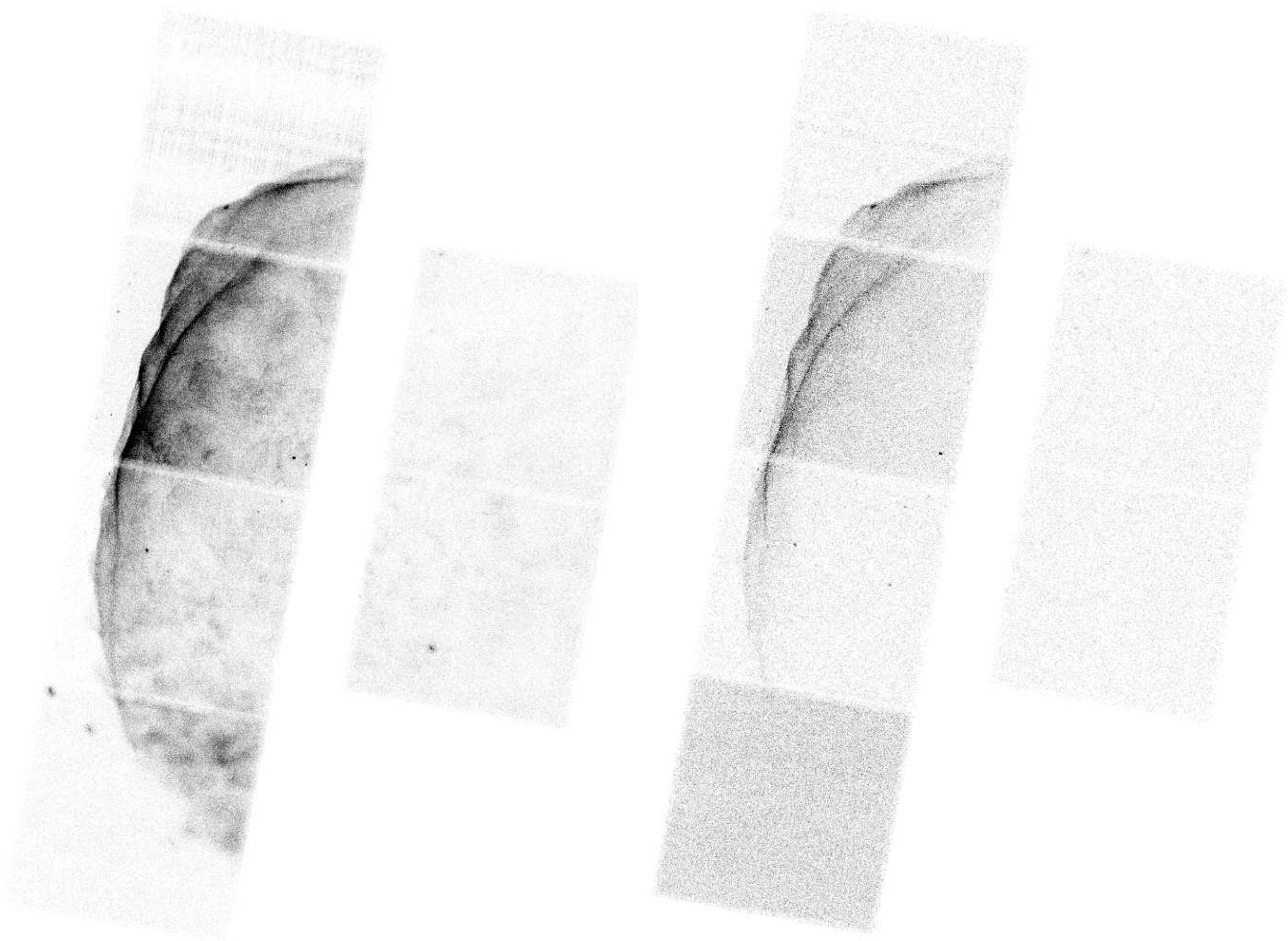

Fig. 1. The images of SN 1006 NE shell binned with 1 arcsec scale, in the 0.5-2.0 keV band (left) and the 2.0–10.0 keV band (right), respectively, both in logarithmic scale.

provided by the pipeline processing at the *Chandra* X-ray Center, we selected *ASCA* grades 0, 2, 3, 4, and 6, as the X-ray events. High energy electrons due to charged particles and hot and flickering pixels were removed. The effective exposure was $\sim$ 68 ks for the observation. In this paper, we concentrated on the data of S3 (BI chip) because this chip has the best efficiency in soft X-rays required for the spectral analyses and its on-axis position provides the best point-spread function required for the spatial analysis.

RESULTS

Image

Figure 1 shows the images for the NE shell of SN 1006. The images are contrasted in the 0.5–2.0 keV band (left) and in the 2.0–10.0 keV band (right) and binned to a resolution of 1 arcsec. The fine spatial resolution of *Chandra* unveils extremely narrow filaments in the hard band. They are running from north to south along the outer edge of the NE shell, parallel to the shock fronts observed by Hα emission line (Winkler & Long 1997). The soft band image, on the other hand, has a larger scale length similar to the *ROSAT* HRI image (Winkler & Long 1997). Many clumpy sub-structures are also seen in this energy band.

Inner Region

To resolve the thermal and non-thermal components, we made a spectrum from a bright clump found in the soft band image, which is located in the inner part of the NE shell (“Inner region” with the dashed ellipse in Figure 1). The background region was selected from a region out of the SNR, as is shown in

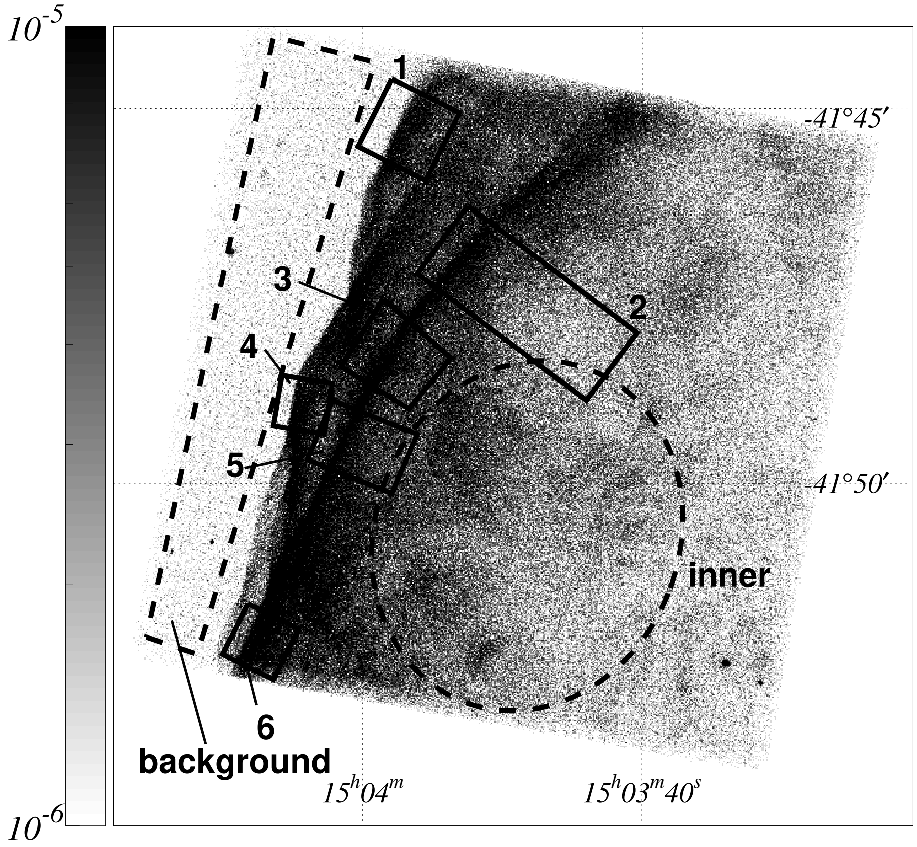

Fig. 2. The close-up view of the 0.5–10.0 keV band image. The gray scale (the left bar) is given logarithmically. The inner and background regions for the spectral analyses and the filament regions for the spatial analyses (No.1–6) are shown with dashed and solid lines, respectively.

Figure 1 with the dashed lines.

The background-subtracted spectrum can be fitted with a thin thermal plasma model in NEI calculated by Borkowski et al. (2001). plus a power-law component. The spectrum of the inner region clump is softer than any other regions in the NE shell, which indicates that the contribution of the thermal component is the largest. Nevertheless the thermal photons are only 0.02% of the non-thermal ones if we limit the energy band to 2.0–10.0 keV (the hard band). Therefore, in the following spatial analyses, we regard that all the photons in the hard band are non-thermal origin.

The Filaments

The outer edge of the NE shell is outlined by several thin X-ray filaments. For the study of these filaments, we selected 6 rectangle regions in Figure 2, in which the filaments are straight and free from other structures like another filament and/or clumps. These regions (solid boxes) are shown in Figure 2 right with the designations of No.1–6 from north to south. Since the SNR shell is moving (expanding) from the right to the left, we call the right and left side as downstream and upstream following the terminology of the shock phenomena.

Figure 3 shows the intensity profiles in the hard (2.0–10.0 keV) with the spatial resolution of 0.5 arcsec, where the horizontal axis (x-coordinate) runs from the east to west (upstream to downstream) along the line normal to the filaments. To estimate the scale length, we define a simple empirical model as a function of position (x) for the profiles;

$$f(x) = \begin{cases} A \exp|\frac{x_0 - x}{w_{\rm u}}| & \text{in upstream} \\ A \exp|\frac{x_0 - x}{w_{\rm d}}| & \text{in downstream,} \end{cases} \qquad (1)$$

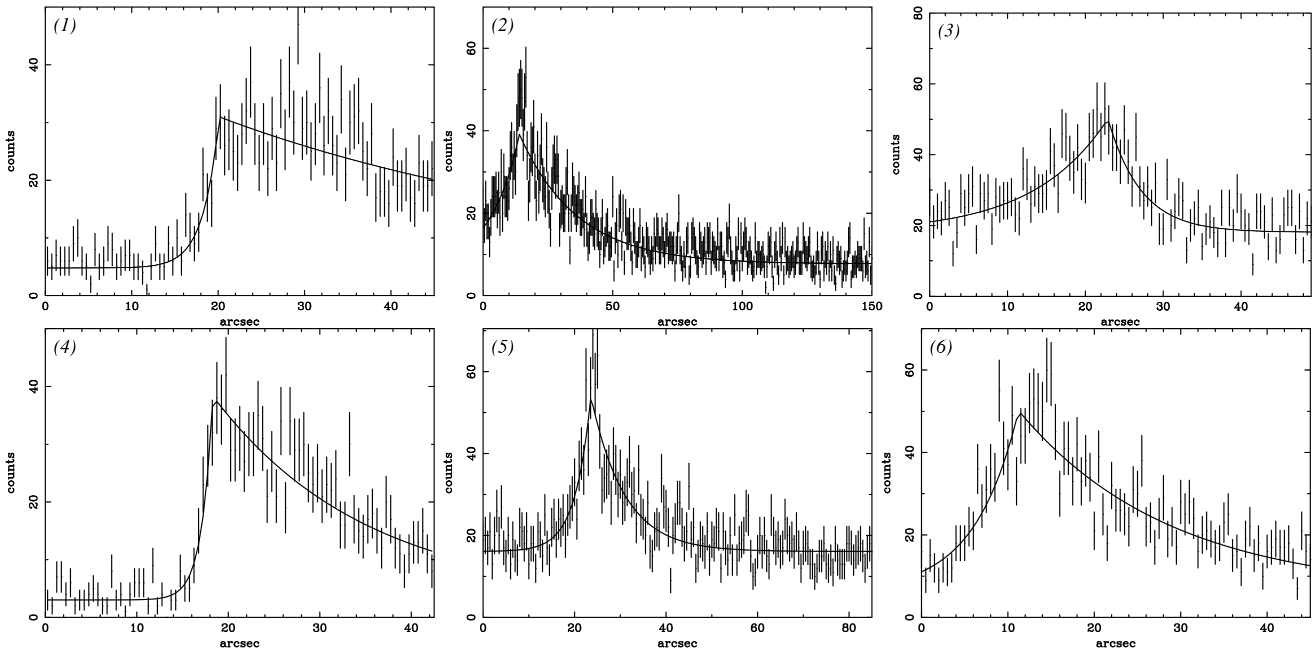

Fig. 3. The profiles of the filaments in SN 1006 NE shell in the 2.0–10.0 keV band.

where A and x_0 are the flux and position at the filament peak. The scale lengths are given by $w_{\rm u}$ and $w_{\rm d}$ for upstream and downstream, respectively. The best-fit models are shown in Figure 3 with the solid lines. The mean and minimum values are 0.04 and 0.01 pc for $w_{\rm u}$ and 0.2 and 0.05 pc for $w_{\rm d}$, respectively.

DISCUSSION

In this section, we interpret the scale length of hard band X-rays, $w_{\rm u}$ and $w_{\rm d}$. For simplicity, we assume the spatial distribution of non-thermal X-rays coincides with that of accelerated electrons. Here, we investigate the observed profiles based on a simple picture of DSA with the magnetic field parallel to the shock normal and compression ratio of about 4, and estimate the physical quantities such as diffusion coefficient, magnetic field, maximum energy of and accelerated electrons. The scale lengths in the upstream side are the projected values of the possible sheet-like structure, hence real lengths should be smaller. We therefore adopted the minimum value of 0.01 pc. For the scale lengths in the downstream side, we used the mean value of 0.2 pc.

We assume that electrons emitting synchrotron X-rays are still accelerating on the shock front. In this condition, the diffusion coefficients in upstream ($K_{\rm u}$) and in downstream ($K_{\rm d}$) are estimated from the relation $w = K/u$ as following;

$$K_{\rm u} \simeq w_{\rm u} \cdot u_{\rm u} = w_{\rm u} \cdot u_{\rm s} = 8.0 \times 10^{24} \quad [{\rm cm^2 s^{-1}}], \tag{2}$$

$$K_{\rm d} \simeq w_{\rm d} \cdot u_{\rm d} = w_{\rm d} \cdot \frac{1}{4} u_{\rm s} = 4.0 \times 10^{25} \quad [{\rm cm^2 s^{-1}}], \tag{3}$$

where the shock speed $u_{\rm s}$ is assumed to be 2600 km s^{-1} (Laming et al. 1996). The acceleration time scale $\tau_{\rm acc}$ is then $\tau_{\rm acc} = \frac{4}{u_{\rm s}^2}(K_{\rm u} + 4K_{\rm d})$ (Drury 1983);

$$\tau_{\rm acc} \simeq 9.7 \times 10^9 \ [{\rm sec}] \ = 310 \ [{\rm years}] \tag{4}$$

The energy loss time scale ($\tau_{\rm loss}$) via synchrotron cooling should be longer than the acceleration time scale of about 300 year, hence using Eq. (4), we obtain;

$$6.3 \times 10^2 B_{\rm d}^{-2} E_{\rm max}^{-1} \geq 9.7 \times 10^9 \quad [{\rm sec}] \tag{5}$$

A probable region in the $E_{\rm max}$–$B_{\rm d}$ space is then limited to the lower side of the dotted line in Figure 4.

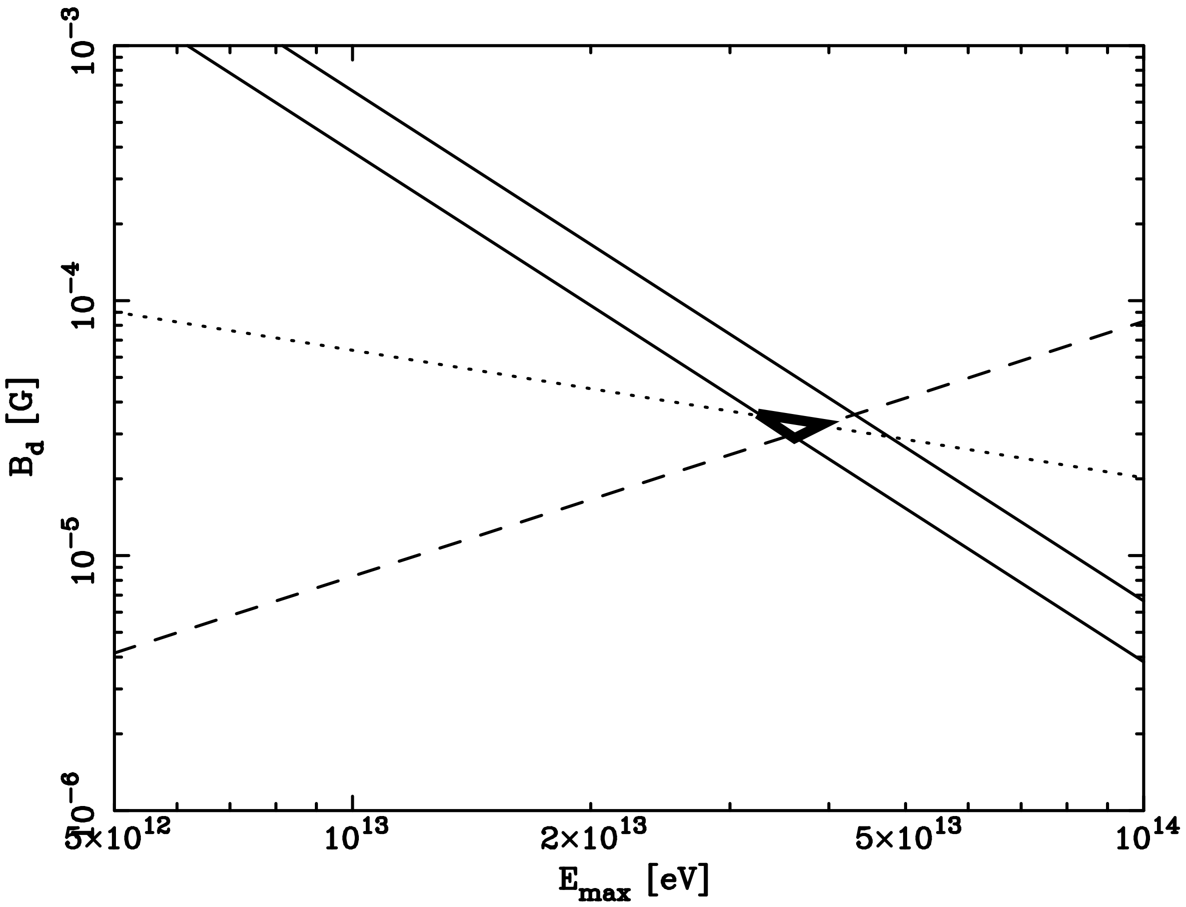

Fig. 4. The relation between $E_{\rm max}$ and $B_{\rm d}$. The solid, dashed, and dotted lines are the relation derived from $E_{\rm rolloff}$, acceleration time scale, and Bohm limit in the filaments. The thick line region is the most probable region for $E_{\rm max}$ and $B_{\rm d}$.

The wide band spectra from X-ray to radio can be fitted with *srcut* model (Reynolds 1998). The best-fit $\nu_{\rm rolloff}$ at the filaments is 2.6 (1.9–3.3)$\times 10^{17}$ Hz, which constrain the maximum energy of electrons $E_{\rm max}$ and magnetic field in downstream $B_{\rm d}$;

$$E_{\rm max} B_{\rm d}^{0.5} = 0.37^{+0.04}_{-0.06} \quad [\text{ergs G}^{0.5}] \tag{6}$$

The allowed region in the $E_{\rm max}$–$B_{\rm d}$ plane is between the two solid lines of Figure 4.

The diffusion coefficient in downstream is given by Skilling (1975) as follows;

$$K_{\rm d} = \frac{1}{3} \xi_{\rm d} \frac{E_{\rm max}}{{\rm e}B_{\rm d}} c \tag{7}$$

The non-dimensional parameter ξ indicates the fluctuation of the magnetic field. The magnetic field strength and its fluctuation become equal at $\xi = 1$ (Bohm limit). The dashed line in Figure 4 is the relation of Eq. (7) for $\xi_{\rm d} = 1$, which should be larger than about one. Therefore, a probable region in the $E_{\rm max}$–$B_{\rm d}$ space is in the upper side of the dashed line.

Using Eq. (5), (6), and (7), we thus constrain the most likely region in the $E_{\rm max}$–$B_{\rm d}$ space to be in the thick lines, where the magnetic field in downstream ($B_{\rm d}$) and the maximum electron energy ($E_{\rm max}$) are in the range of 30–40 μG and 30–40 TeV, respectively. The small $\xi_{\rm d}$ (the likely region is $1 \leq \xi_{\rm d} \leq 1.3$) indicates that the magnetic field is highly turbulent.

From Eq.7, the ratio of the diffusion coefficient ($\frac{K_{\rm u}}{K_{\rm d}}$) is given by $\frac{\xi_{\rm u} B_{\rm d}}{\xi_{\rm d} B_{\rm u}}$. Observationally, the ratio is about 0.2 (from Eq.2 and 3), we thus obtain the relation of magnetic field and ξ between upstream and downstream as

$$\frac{\xi_{\rm u}}{\xi_{\rm d}} \sim 0.2 \frac{B_{\rm u}}{B_{\rm d}} \tag{8}$$

Since $\frac{B_{\rm u}}{B_{\rm d}}$ varies between $\frac{1}{4}$ and 1 under the assumption of the strong shock with compression ratio of about 4, depending on the shock obliqueness, $\xi_{\rm u}$ is in the range of 0.05–0.3. Our result reconciles with a picture of a conventional DSA with the magnetic field parallel to the shock normal.

A possible scenario for this extremely small diffusion length in upstream is perpendicular field to the shock normal in this region. In downstream on the other hand, the shock flow may compress and partly stretches the magnetic field in the radial direction, which produces highly disordered field with small fraction of radial component. This scenario is consistent with the radio polarization data in the NE shell by Reynolds & Gilmore 1993). Since the current radio polarization data are spatially poor and limited mainly to the downstream region, fine structure observations, particularly at the very narrow region in the upstream side should be crucial. The DSA process can explain marginally the observation result. However, we point out that another acceleration mechanism may exist, which can explain observed thin non-thermal filament. Hoshino & Shimada (2002) proposed the electron shock surfing acceleration mechanism. More quantitative study is necessary, whether the mechanism can accelerate particles up to 30 TeV in this system and whether the accelerated particles have the power-law spectrum.

ACKNOWLEDGEMENTS

Our particular thanks are due to M. Hoshino, T. Terasawa, T. Yoshida, and S. Inutsuka for their fruitful discussions and comments. We also thank the anonymous referee for helpful comments. A.B. and M.U. are supported by JSPS Research Fellowship for Young Scientists.

REFERENCES

Bell, A.R. 1978, MNRAS, 182, 443

Borkowski, K.J., Lyerly, W.J., & Reynolds, S.P. 2001, ApJ, 548, 820

Drury, L.O'C. 1983, Rep. Prog. Phys., 46, 973

Hoshino M., Shimada N. 2002, ApJ, 572, 880

Koyama, K., Petre, R., Gotthelf, E.V., Hwang, U., Matsura, M., Ozaki, M., & Holt S.S. 1995, Nature, 378, 255

Laming, J. M., Raymond, J. C., McLaughlin, B. M., & Blair, W. P. 1996, ApJ, 472, 267

Skilling, J. 1975, MNRAS, 172, 557

Weisskopf, M.C., O'dell, S.L., & van Speybroeck, L.P. 1996, *Proc. SPIE*, 2805, 2

Winkler, P.F. & Long, K.S. 1997, ApJ, 491, 829